Solid Molybdenum Nitride Microdisc Electrodes: Fabrication, Characterisation, and Application to the Reduction of Peroxodisulfate

Saiful Arifin Bin Shafiee, Andrew L. Hector, Guy Denuault*

Chemistry, University of Southampton, Southampton, SO17 1BJ, UK.
Email: gd@soton.ac.uk

Abstract

A new methodology was developed to fabricate solid molybdenum nitride microdisc electrodes for the first time. The MoN microrods were produced by heating Mo microwires in dry NH_3 atmosphere for several hours. They were characterised by scanning electron microscopy (SEM), energy dispersive spectroscopy (EDS) and X-ray diffraction (XRD). The latter revealed the samples had crystallised in the δ_3-MoN phase with a core of γ-Mo_2N. Their electrochemical behaviour was probed for the reduction of $Ru(NH_3)_6^{3+}$. For this fast electron transfer the MoN microdisc electrodes returned similar voltammetric features to Pt microelectrodes. Their amperometric response was further tested with the reduction of peroxodisulfate. In contrast with other electrode materials, the reduction of $S_2O_8^{2-}$ on MoN microdiscs delivered steady state voltammograms with well-defined diffusion controlled plateau. At low sweep rates, the limiting current was consistent with hemispherical diffusion and stable for at least 500 s. The diffusion coefficient of $S_2O_8^{2-}$ derived from these results, 9.5×10^{-6} cm^2 s^{-1}, is in excellent agreement with previous work. At high sweep rates, the reduction of peroxodisulfate was found to be complicated by the simultaneous reduction of adsorbates. The results indicate that MoN is an ideal electrode material to monitor the concentration of peroxodisulfate under steady state conditions.

Keywords: Molybdenum nitride; Microelectrodes; Peroxodisulfate.

1.0 Introduction

The electrochemical behaviour of metal nitrides, MoN included, has not been widely studied. Amorphous films of CoN have been found to have good properties for the oxygen reduction reaction (ORR) but are unfortunately unstable near the ORR onset potential [1, 2]. MoN materials are typically prepared as thin films [3, 4] with thicknesses ranging from 0.5 to 20 μm and are usually made via physical vapour deposition [5, 6] or chemical vapour deposition [7, 8]. Thin film MoN electrodes have been examined by a few groups [8-11] but in most cases the electrodes were used as capacitors or as electrocatalysts for the oxygen reduction reaction (ORR) [7, 9, 12]. During fabrication and use these films often crack and delaminate [13] thereby producing higher surface areas and exposing the underlying substrate. In this paper, we demonstrate the viability of producing solid MoN microelectrodes which do not suffer these limitations. In brief, we prepare MoN microelectrodes from Mo microwires via ammonolysis and after characterisation we exploit them for electroanalytical purposes. In particular we investigate the electroreduction of peroxodisulfate ($S_2O_8^{2-}$) which has complicated voltammetry on common electrode materials [14, 15]. We show that on MoN microdiscs the reduction of $S_2O_8^{2-}$ can be diffusion-controlled without having to modify the electrode surface.

Molybdenum nitride exists in many structural forms. α-MoN_x is Mo metal with small amounts of interstitial N [16]. γ-Mo_2N adopts the cubic rocksalt structure with around 50% vacancies on the anion sites, and β-MoN is a tetragonal distortion of the γ-Mo_2N with N atoms displacements [16, 17]. Different phase constituents can be obtained by controlling parameters including the temperature during the synthesis [3]. For example, β-MoN is stable at low temperature and γ-MoN is stable at high temperature [17]. There are several types of hexagonal (δ-) MoN [17]. δ_1-MoN consists of a WC-type crystal lattice with stacking faults of the N atoms layers along the *c*-axis. δ_2-MoN has a NiAs type structure and δ_3-MoN can be

described as a slightly distorted NiAs superstructure. Mo_5N_6 is the outcome of coalescence of WC- and NiAs-type building blocks with vacancies on Mo sites. In this work, several characterisations were performed on the MoN samples before recording their electrochemical response. Little is known about their electrochemistry but Cao *et al.* reported that δ-MoN is a better ORR catalyst than the γ-Mo_2N phase [12].

Peroxodisulfate, also known as peroxydisulfate and persulfate, is a strong oxidising agent which has been used to decompose organic compounds [18], particularly in wastewaters. According to Botukhova and Petrii, the peculiar voltammetry of $S_2O_8^{2-}$ was first reported in 1949 [15]. Many electrode materials have been employed over the years, either pristine or modified surfaces, to further understand the electrochemical behaviour of $S_2O_8^{2-}$. Some of the materials include polycrystalline Au [14], single crystals of Au [19, 20], roughened Au [21], Pt [15], bismuth modified Pt [15, 22], cadmium and lead modified Pt [23], thallium modified Pt [24], Prussian blue modified Pt [25], modified carbon nanotubes [26], and boron-doped diamond [27]. Most of the studies were conducted using rotating disc electrodes (RDE). In this work, we have employed microelectrodes which are known to have high mass transfer coefficient, low ohmic drop, and low double layer charging current [28].

Although the diffusion-controlled reduction of $S_2O_8^{2-}$ has been reported, in most cases the RDE voltammograms are poorly-defined and only reach a limiting current in a narrow potential window. To the best of our knowledge, the only materials that demonstrate sigmoidal shape RDE voltammograms are the bismuth and lead-modified Pt electrodes [15, 22, 23]. In all cases the stability of the amperometric response is not mentioned.

Overall the reduction of $S_2O_8^{2-}$ is a two-electron process [21]:

$$S_2O_8^{2-} + 2\,e^- \rightarrow 2\,SO_4^{2-} \qquad \textbf{(}\text{Eq. 1)}$$

However the reaction mechanisms proposed to explain its voltammetry are complex and generally involve dissociative chemisorption of an intermediate. For example the mechanism proposed by Samec and co-workers for the reduction of $S_2O_8^{2-}$ on gold involves two pathways [14]. The first occurs at more positive potentials and involves the fast dissociative chemisorption of intermediates followed by their reduction in a slow one-electron process:

$$S_2O_8^{2-} \rightarrow (S_2O_8^{2-})_{ads} \rightarrow 2(SO_4^{-})_{ads} \quad \text{(Eq. 2)}$$

$$(SO_4^{-})_{ads} + e^{-} \rightarrow (SO_4^{2-})_{ads} \rightarrow SO_4^{2-} \quad \text{(Eq. 3)}$$

while the second occurs at more negative potentials and involves two consecutive one-electron transfers:

$$S_2O_8^{2-} + e^{-} \rightarrow SO_4^{2-} + SO_4^{-} \quad \text{(Eq. 4)}$$

$$SO_4^{-} + e^{-} \rightarrow SO_4^{2-} \quad \text{(Eq. 5)}$$

Whatever the electrode material, it is clear that the adsorption process complicates the mechanism and it is of interest to find a material that can promote the mass transport controlled reduction of peroxodisulfate.

We first report the fabrication and characterisation of the MoN microdisc electrodes then present their electrochemical behaviour with a model redox compound before discussing the electrochemistry of peroxodisulfate.

2.0 Experimental

A 25 μm diameter Mo wire (99.95%, Advent Research Materials) was cut into several 5 mm long pieces. The wires were then laid in between two alumina tiles to prevent them from bending or curling during the ammonolysis. The tiles were placed in the middle of a silica tube located inside a programmable tube furnace (Lenton Thermal Designs Limited).

Dry ammonia gas (BOC anhydrous grade, further dried with molecular sieves) was flowed through the sample tube during the entire nitridation process. The temperature was raised (10 ^{o}C min^{-1}) to 800 ^{o}C, held at this value for 60 hours, raised (10 ^{o}C min^{-1}) to 1100 ^{o}C, held at this value for 30 hours, decreased (10 °C min^{-1}) to 800 ^{o}C and held at this value for a further 15 hours. The sample was left to cool to room temperature under ammonia then flushed with nitrogen for 15 min to remove excess ammonia. The SEM images and the EDS spectra of the samples were acquired using a Phillips XL 30 ESEM with a Thermofisher Ultradry detector. The XRD analysis was performed using a Rigaku SmartLab diffractometer with Cu-K_{α} radiation and a DTex-250 1D detector. XRD patterns were collected in transmission mode with a 0.2 mm line beam and the samples glued to a Scotch Magic tape (3M), or with a 0.1 mm spot on a polished microelectrode cross-section. The XRD data was analysed and treated using the PDXL2 software. Rietveld refinement was carried out using the GSAS package [29] with model structures from the Inorganic Crystal Structure Database [30].

To fabricate the MoN microdisc electrodes, one end of the MoN wire was connected to a copper wire (RS Components) using silver epoxy (RS Components). A 1 mL pipette tip (Diamond) was bisected and covered with Teflon tape then used as a mould for the electrode fabrication. A small amount of epoxy resin (Araldite) was deposited inside the mould. The wire was laid on top of the epoxy resin before adding more epoxy resin to completely cover the wire. The epoxy was allowed to harden overnight thus providing a solid insulating sheath to the otherwise brittle MoN wires. The hardened epoxy was polished with silicon carbide papers (Starke) of different grades (200, 600, and 1200) to expose the MoN microdisc. The electrode was then polished with alumina lapping films (3M) of different grades (5, 1 and, 0.3 μm) to obtain a mirror finished surface. The electrode surface was cleaned using a wetted microcloth (Buehler) and deionised water.

All chemicals were used as received without further purification. The $K_2S_2O_8$ (≥ 99 %) and KCl (≥ 99 %) were obtained from Fluka and Fisher Scientific respectively. The $Ru(NH_3)_6Cl_3$ (98 %) and $KClO_4$ (≥99.99%) were both obtained from Aldrich. The deionised water (resistivity 18.2 MΩ cm) was acquired from a Purite Select water purification system to prepare the aqueous solutions and to clean the glassware. The glassware was soaked in Decon 90 (BDH) overnight. It was then rinsed with copious amounts of deionised water before being dried in an oven (LTE Scientific) at 40 - 50 ºC before use. Five-neck cells were used to hold the test solutions. The electrochemical experiments were conducted inside a grounded Faraday cage to reduce the electromagnetic noise and performed using an Autolab PGSTAT101 controlled with NOVA 1.10, both from EcoChemie. The experiments were conducted at room temperature (19 – 23 ºC). The test solutions were thoroughly deoxygenated with Ar gas (BOC) for 30 min, then for 15 min before recording the voltammetric responses. To maintain reproducibility, the electrode was polished for 10 min with 0.3 μm alumina lapping film to expose a pristine MoN surface before each experiment.

3.0 Results and discussion

3.1 Material characterisation

XRD was performed on the MoN samples to determine the phase produced during ammonolysis. Figure 1 shows a Rietveld fit to a typical diffraction pattern obtained with the MoN wires in transmission mode. The broad background arises from the Scotch tape used to mount the fragile wires in the beam (see figure SI1 for a spectrum of the background). The δ_3-MoN phase (lattice parameters a = 0.574(3) and c = 0.563(3) nm) accounts for most of the observed intensity, with a small fraction of γ- Mo_2N also observed. The lattice parameters of the δ_3-MoN phase are very close to the literature values of 0.574 and 0.562 nm for that phase[31]. It is common to observe some cubic γ-Mo_2N in hexagonal δ_3-MoN [31], however here the hexagonal δ_3-MoN phase clearly dominates. Using a microfocus beam to collect a

pattern on a polished cross-section, figure SI2, the contribution from the γ-Mo_2N phase is stronger, showing that this phase is present mainly in the core of the wires, with δ_3-MoN dominant in the shell. Of course, by polishing through the wires to make microelectrodes we are exposing both regions.

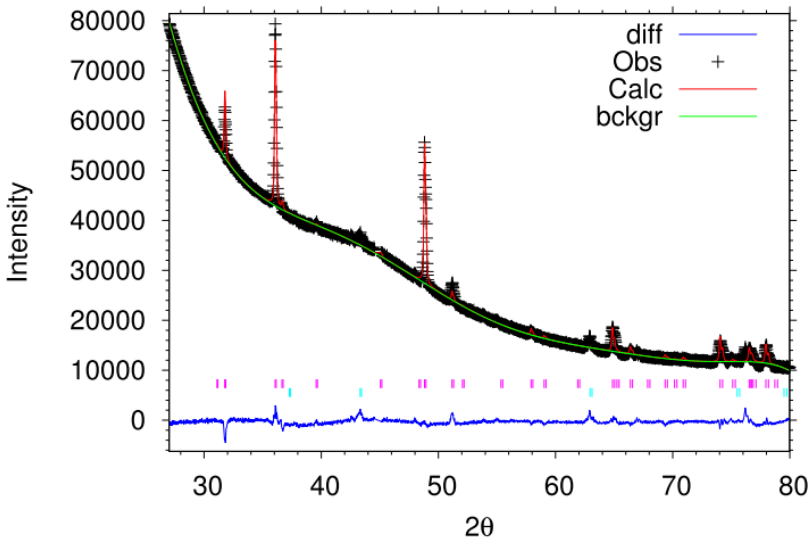

Figure 1: Rietveld fit (R_{wp} = 1.8 %, R_p = 1.2 %) to the XRD pattern of a MoN microwire. Crosses mark the data points, the red line the fit, the green line the background and the blue line the difference (data-model). Tick marks show the allowed reflection positions for the δ_3-MoN (cyan, space group *P*6$_3$mc) and γ-MoN (pink, space group *Fm-3m).* A small peak at 44.8º could not be accounted for, and was excluded from the fit.

Figure 2 shows the SEM images obtained on the MoN and Mo wires. Typical EDS spectra are shown in figure SI3. The Mo wires were originally striated, figure 2, but the nitridation process caused their surface to become grainy and rougher. This is probably what led to the rough edges seen on the microdiscs, figure SI4. Kim *et al*. [13] reported that this was due to the volumetric enlargement of the crystal grains throughout the ammonolysis. Strong Mo and N peaks can be seen on the EDS spectrum of the MoN wire, figure SI3. The ratio of Mo to N obtained is 1:0.7. As expected, the N peak is absent from the EDS spectrum of the Mo wire. The strong carbon peaks are due to the carbon tab used to mount the sample. Although some surface oxidation can also be expected [5], the oxygen peak is mainly due to

the wet SEM mode (a low vapour pressure of water) used to collect the data; this imaging mode is needed because of the large area of epoxy.

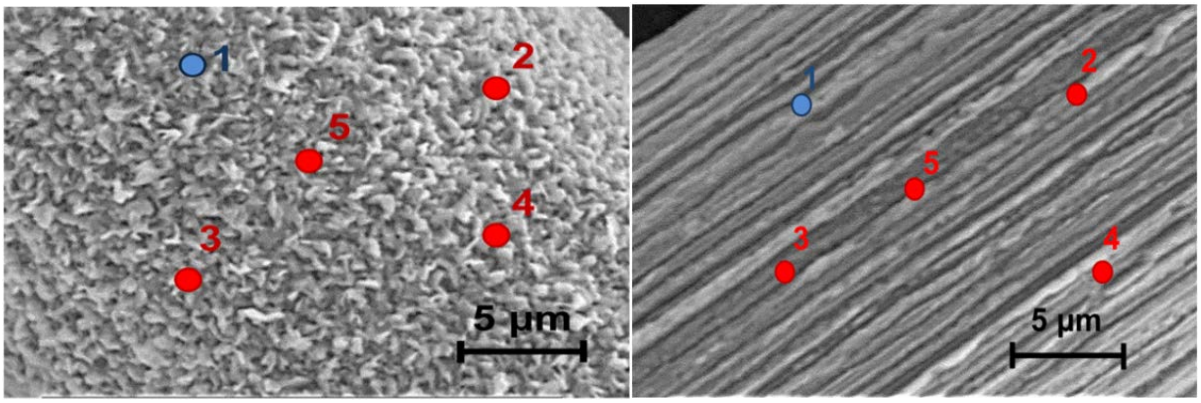

Figure 2: SEM images taken on the side of δ_3-MoN (left) and Mo (right) wires. The EDS analysis was conducted at five different and random locations (numbered spots) on the wires. The representative EDS spectra (blue spots) are shown in fig. SI3. Conditions: 5000x magnification, 5 kV, gaseous secondary electron detector, and wet mode.

3.2 Voltammetry

The electrochemical behaviour of the freshly polished MoN microdisc electrode was first probed with the reduction of $Ru(NH_3)_6^{3+}$, a simple redox process known to be a fast outer sphere electron transfer. The cyclic voltammogram of the MoN microdisc electrode was then compared to that recorded with a similar size Pt microdisc, figure 3.

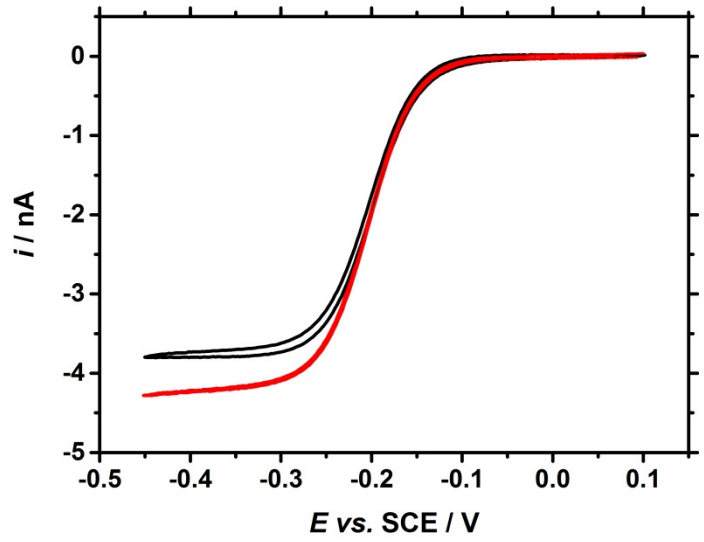

Figure 3: Cyclic voltammograms recorded at 2 mV s^{-1} with a 26 µm Ø MoN (red) and a 25 µm Ø Pt (black) microdisc in deoxygenated 1 mM $Ru(NH_3)_6Cl_3$ + 0.5 M KCl.

Matching sigmoidal steady state cyclic voltammograms consistent with hemispherical diffusion were obtained with both electrodes. The redox wave occurs at the same potential in both cases; this indicates that the reduction of $Ru(NH_3)_6^{3+}$ is not affected by the MoN surface. The hysteresis between the forward and reverse scans of the voltammogram obtained with the MoN microdisc is noticeably small; this suggests that the MoN surface was very clean. The limiting current taken at -0.4 V *vs.* SCE is in very good agreement with the theoretical value estimated from the following equation [32]:

$$i_{\mathrm{lim}} = 4nFDCa \qquad \text{(Eq. 6)}$$

where n is the number of electrons transferred (1), F the Faraday constant, D the diffusion coefficient of $Ru(NH_3)_6^{3+}$ in this medium (8.4×10^{-6} cm^2 s^{-1}) [33], C its concentration in the bulk, and a the radius of the electrode. The shape of the voltammogram recorded with the MoN electrode was examined by plotting E vs. ln ($i_{\mathrm{lim}} - i$) / i with the potential and current values taken from the declining part of the wave (figure SI5 left). The plot, figure SI5 (right), yields a straight line, which was analysed with the equation for the steady state voltammetry of reversible processes [32]:

$$E = E_{1/2} + \frac{RT}{nF}\ln\left(\frac{i_{\mathrm{lim}} - i}{i}\right) \qquad \text{(Eq. 7)}$$

where E is the applied potential, $E_{1/2}$ the half-wave potential, i_{lim} the limiting current, and i the experimental current at E. R, T and F have their usual meaning. In both cases the fitted slope, Table 1, is very close to RT/F. This confirms that the reaction is reversible with both electrodes and implies that the MoN electrode behaves like Pt for the reduction of $Ru(NH_3)_6^{3+}$.

Table 1: Comparison of the voltammetric features obtained with the MoN and Pt microdisc electrodes for the reduction of $Ru(NH_3)_6^{3+}$.

Electrode material	Voltammetric feature	
	Slope / V	**$E_{1/2}$ / V**
Pt	0.026	-0.199
MoN	0.026	-0.203

To assess the electrochemical properties of MoN further we chose to investigate the reduction of the peroxodisulfate anion. On most common electrode materials [14, 15, 20-22, 27] this reaction yields very poor voltammetry. The voltammograms have complicated hysteresis and the current barely reaches diffusion control, figure SI6. The MoN microdisc electrodes were polished with a 0.3 micron alumina lapping film and thoroughly cleaned before each experiment. Figure 4 shows the voltammetric response obtained with the MoN microdisc electrode in presence and absence of $K_2S_2O_8$.

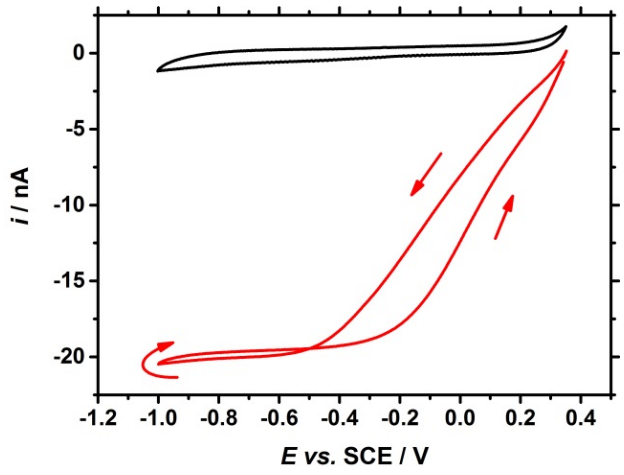

Figure 4: Cyclic voltammograms recorded at 10 mV s^{-1} with a 26 µm Ø MoN microdisc electrode in deoxygenated 0.1 M $KClO_4$ without (black) and with (red) 2 mM $K_2S_2O_8$.

The reduction starts near the onset of solvent oxidation, +0.35 V, and no attempt was made to start the sweep from higher potentials. The wave is drawn out but it reaches a clear

plateau in both scan directions and its limiting current is close to the theoretical value (-19.5 nA) estimated with eq. 6 taking the diffusion coefficient of $S_2O_8^{2-}$ as 9.7×10^{-6} cm^2 s^{-1} [14]. A crossover point can be seen on the cyclic voltammogram recorded in the presence of $S_2O_8^{2-}$ and a 2nd cross over point is expected circa +0.4 V. Between -0.5 and +0.35 V the reaction visibly runs a lot faster on the reverse scan than on the forward scan. This behaviour is also observed for the reduction of $S_2O_8^{2-}$ on Au [14, 21, 34], Ni [21], and Pt [15]. Such hysteresis is typically seen for the oxygen reduction reaction [35, 36] and is characteristic of processes where adsorbed intermediates compete with other adsorbates for the adsorption sites. The voltammogram therefore suggests that the MoN surface had more vacant sites on the reverse sweep than on the forward sweep. This presumably results from the removal of Mo oxides during the negative scan, although there is no obvious voltammetric feature on the background voltammogram, figure 4, even when recorded at high sweep rate, figure 5.

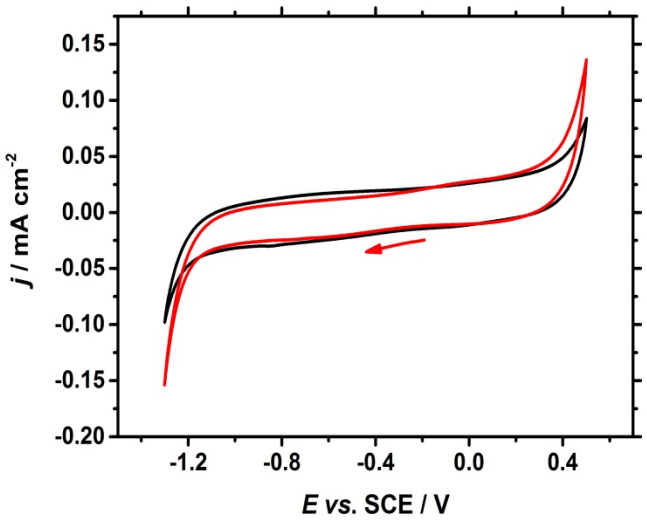

Figure 5: Cyclic voltammograms (1st cycle) recorded at 100 mV s^{-1} with a 27 µm Ø (black) and a 28 µm Ø (red) MoN microdisc in deoxygenated 0.5 M KCl. The potential was swept negatively starting at -0.1 (black) & 0.02 (red) V.

The reduction of peroxodisulfate was recorded over a range of sweep rates, figure SI7. Between 10 and 100 mV s^{-1} the voltammograms retain a sigmoidal shape. This shape disappears above 100 mV s^{-1} and a reduction peak whose magnitude increases with scan rate

appears circa -0.6 V. Between 100 mV s^{-1} and 1 V s^{-1} the hysteresis between the forward and reverse sweeps increases but the crossover points are visible up to 2 V s^{-1}. At higher scan rates the reduction peak increases systematically but there is no corresponding oxidation peak on the reverse sweep. Furthermore the reduction peak does not present the characteristic shape of a diffusion controlled process. The influence of sweep rates on the shape of microdisc voltammograms is complicated because of the transition from hemispherical diffusion at low sweep rates to planar diffusion at high sweep rates. To analyse the reduction of peroxodisulfate we plotted the maximum current measured on the forward sweep against the square root of sweep rate, figure 6. Initially the maximum current is independent of the sweep rate and this is consistent with hemispherical diffusion. As mentioned previously this current matches the theoretical limiting current calculated with equation 6. The maximum current starts to increase above 20 mV s^{-1} and above 2 V s^{-1} it appears proportional to the square root of the sweep rate. In principle this should be consistent with planar diffusion however the currents obtained at high sweep rates are much larger than expected for a purely diffusion controlled current as estimated using the equation derived by Aoki *et al.* [37] for a microdisc, figure 6. This suggests the presence of an additional current arising from another process. Because this extra current is only visible at short time scales we speculate that it arises from the reduction of adsorbed species which bound to the surface upon exposure to peroxodisulfate. This is supported by the following observation: a voltammogram recorded in $KClO_4$ with an electrode previously immersed in $K_2S_2O_8$ shows significant extra current on the first cycle compared to the same experiment conducted with a pristine electrode not exposed to the peroxodisulfate solution, figure 7. The extra current appears below -0.5 V, the same potential region as the peroxodisulfate reduction plateau. Interestingly, the extra current decreases on subsequent cycles but does not disappear completely even though the voltammogram is recorded in a solution devoid of $K_2S_2O_8$. Further analysis of the data in

figure 6 reveals that the extra current (the difference between the maximum current recorded and the theoretical value expected under diffusion control) increases linearly with scan rate and not with its square root (insert in figure 6). This therefore rules out the involvement of a diffusing species and supports the assignment of the extra current to the reduction of a surface bound species. So the overall current observed is not proportional to the square root of the scan rate as may seem at first glance. Hence exposure of the MoN surface to a solution of peroxodisulfate leaves strongly bound adsorbates which can only be removed by polishing the electrode, figure 7. These adsorbates can be reduced during potential cycling but not electrochemically removed from the surface. For this reason the reduction of peroxodisulfate only appears diffusion controlled at sweep rates sufficiently low for the reduction current of the adsorbed species to be negligible.

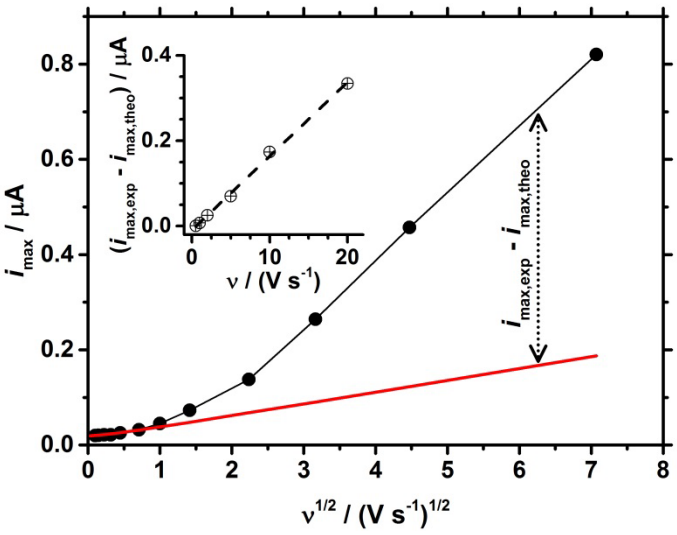

Figure 6: Scan rate dependence of the maximum currents (black symbols) taken on the forward sweeps of the voltammograms shown in figure SI7. They were recorded with a 26 µm Ø MoN microdisc electrode in 2 mM $K_2S_2O_8$ + deoxygenated 0.1 M $KClO_4$. The red line corresponds to the theoretical maximum current calculated with equation 10 in [37] using n = 2, D = 9.5×10^{-6} cm^2 s^{-1}, c = 2 mM and a = 13 µm. The insert shows the scan rate dependence of the difference between experimental and theoretical maximum currents (symbols) and the line of best fit (dashed line).

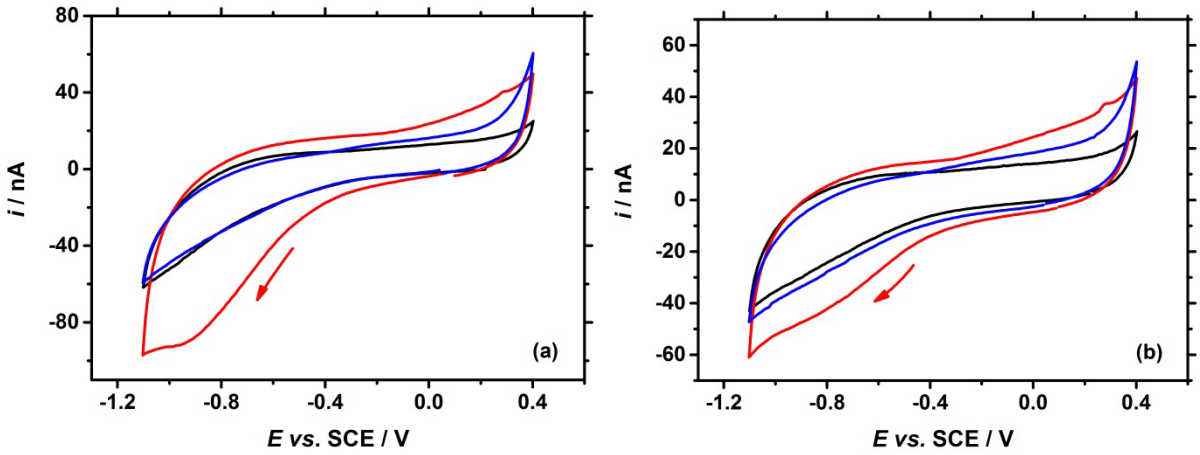

Figure 7: Voltammograms (a: 1st cycle, b: 3rd cycle) recorded with a 26 µm Ø MoN disc at 5 V s^{-1} in 0.1 M $KClO_4$. The sweeps started at the OCP, ~0.1 V. (black) recorded before immersing the electrode in $K_2S_2O_8$. (red) obtained after immersing the electrode in 2 mM $K_2S_2O_8$ for 25 min. (blue) recorded after repolishing for 10 min.

Cyclic voltammograms were also recorded in different concentrations of $S_2O_8^{2-}$ to assess whether the limiting current was proportional to concentration as predicted by eq. 6. Above 20 µM the limiting currents show a linear relationship with the concentrations of $S_2O_8^{2-}$, figure 8. Below 20 µM the current increases with the concentration but there is no obvious linear response. From the linear region in figure 8 the diffusion coefficient of peroxodisulfate is estimated to be 9.5×10^{-6} cm^2 s^{-1} which is in excellent agreement with the literature [14]. Chronoamperometry, figure 9, reveals that the limiting current is remarkably stable for a long time.

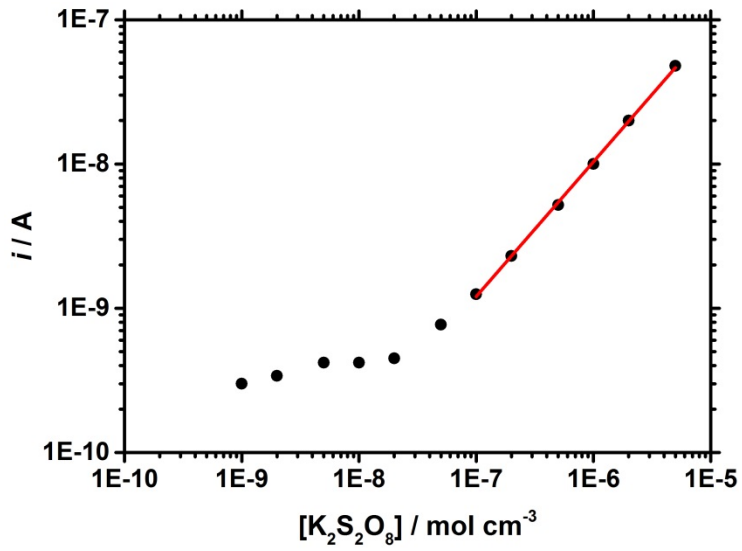

Figure 8: Limiting currents taken at -0.6 V vs. SCE as a function of the concentration of $K_2S_2O_8$ in deoxygenated 0.1 M $KClO_4$ from voltammograms recorded at 10 mV s^{-1} with a 26 µm Ø MoN microdisc, Figure SI8.

The results suggest that the MoN surface promotes the reduction of peroxodisulfate over a wide potential window. Although non-ideal, the steady state voltammograms do not suffer the distortions observed with macro- and microelectrodes made with other materials and steady state conditions can be exploited to monitor the concentration of peroxodisulfate. Here the solid MoN microdiscs have a key advantage in that their surface does not need modification or pre-treatment except for polishing before experiments. At short times however, complications arise from the reduction of irreversibly adsorbed peroxodisulfate anions (or other species resulting from their dissociative adsorption).

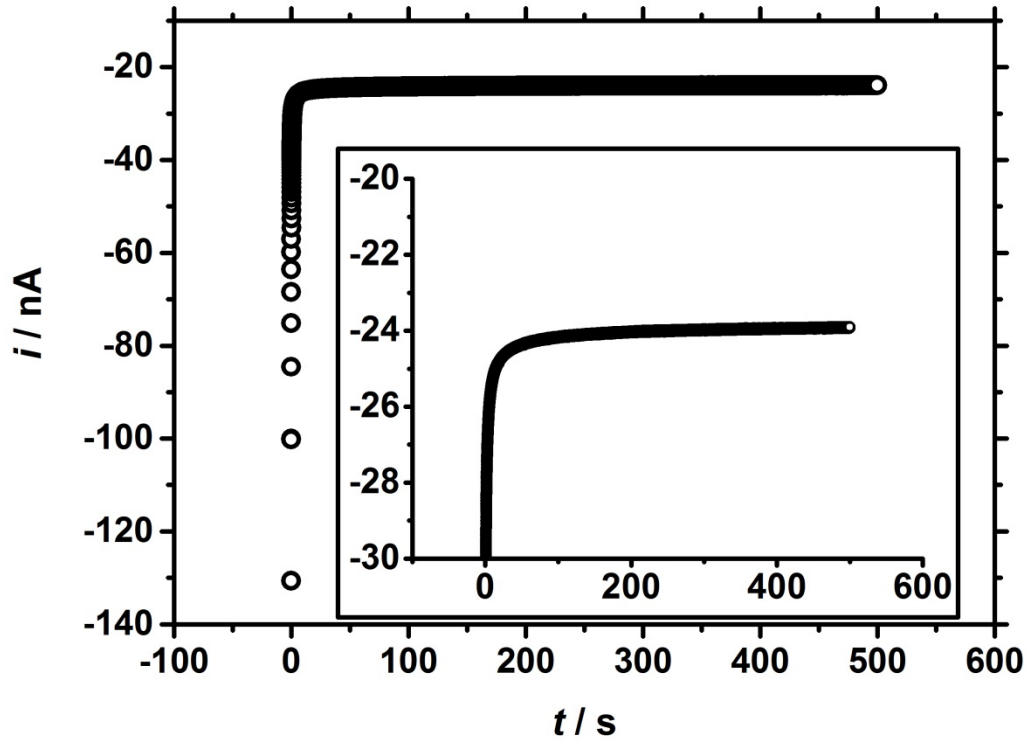

Figure 9: Chronoamperogram recorded with a 29 µm Ø MoN microdisc electrode in 2 mM $K_2S_2O_8$ + deoxygenated 0.1 M $KClO_4$. The potential was stepped from 0.3 V to -0.8 V *vs.* SCE and held there for 500 s. The inset shows the same chronoamperogram but between -30 and -20 nA.

4. Conclusion

Solid MoN microwires were successfully prepared via nitridation. Their surface appears rough under SEM but the microdiscs produced by exposing their cross section after sealing in epoxy were sufficiently robust to be polished repeatedly. EDS spectra showed strong Mo and N peaks while XRD analysis indicated the wires were consistent with solid δ_3-MoN with some γ-Mo_2N at the core. When tested in presence of a fast redox couple the discs produced diffusion controlled voltammograms similar to that at a Pt microdisc of comparable size. Unlike Pt and all other materials tested the MoN microdiscs produced diffusion controlled limiting currents for the reduction of $S_2O_8^{2-}$ over a wide potential window. Steady state voltammograms consistent with hemispherical diffusion of $S_2O_8^{2-}$ were obtained at low scan rates but at higher scan rates the voltammetry was complicated by the reduction of adsorbed species and the currents recorded were much larger than predicted assuming a pure

diffusion controlled process. The limiting current was found to be stable and proportional to $S_2O_8^{2-}$ concentrations above a few micromoles. Solid MoN is the only material we found that produced a stable and diffusion controlled limiting current to monitor the reduction of $S_2O_8^{2-}$ with a bare microelectrode. In contrast to thin films, the solid electrode can be reliably polished to expose a fresh surface of MoN before each experiment. We are investigating whether solid MoN microelectrodes can be exploited for other redox processes.

5. Acknowledgement

SABS would like to thank Majlis Amanah Rakyat (Malaysia) for their sponsorship. The authors also thank EPSRC for funding the SmartLab diffractometer under EP/K00509X/1 and EP/K009877/1.

6. References

[1] M. Azuma, M. Kashihara, Y. Nakato, H. Tsubomura, Reduction of Oxygen to Water on Cobalt-Nitride Thin-Film Electrodes Prepared by the Reactive Rf Sputtering Technique, J. Electroanal. Chem., 250 (1988) 73-82.

[2] A. Ishihara, H. Imai, K.-i. Ota, Transition Metal Oxides, Carbides, Nitrides, Oxynitrides, and Carbonitrides for O_2 Reduction Reaction Electrocatalysts for Acid PEM Fuel Cells, in: Z. Chen, J.P. Dodelet, J. Zhang (Eds.) Non-Noble Metal Fuel Cell Catalysts, Wiley-VCH Verlag GmbH & Co. KGaA, Weinheim, 2014, pp. 183-204.

[3] Proceedings of the Symposium on Electrochemical Capacitors II, The Electrochemical Society, Inc., Paris, 1997.

[4] X. Zhong, L. Liu, Y. Jiang, X.D. Wang, L. Wang, G.L. Zhuang, X.N. Li, D.H. Mei, J.G. Wang, D.S. Su, Synergistic Effect of Nitrogen in Cobalt Nitride and Nitrogen-Doped Hollow Carbon Spheres for the Oxygen Reduction Reaction, Chemcatchem, 7 (2015) 1826-1832.

[5] T. Suszko, W. Gulbiński, J. Jagielski, The role of surface oxidation in friction processes on molybdenum nitride thin films, Surface and Coatings Technology, 194 (2005) 319-324.

[6] V.V. Atuchin, T. Khasanov, V.A. Kochubey, L.D. Pokrovsky, T.A. Gavrilova, Structural and optical properties of gamma-MO2N thin films deposited by DC reactive magnetron sputtering, International Journal of Modern Physics B, 23 (2009) 4817-4823.

[7] T.C. Liu, W.G. Pell, B.E. Conway, S.L. Roberson, Behavior of molybdenum nitrides as materials for electrochemical capacitors - Comparison with ruthenium oxide, J. Electrochem. Soc., 145 (1998) 1882-1888.

[8] S.L. Roberson, D. Evans, D. Finello, R.F. Davis, Growth and electrochemical characterization of single phase MoxN films for the fabrication of hybrid double layer capacitors, in: D.S. Ginley, D.H. Doughty, B. Scrosati, T. Takamura, Z.M.J. Zhang (Eds.) Materials for Electrochemical Energy Storage and Conversion, Li-Batteries, Capacitors and Fuel Cells, Materials Research Society, Warrendale, 1998, pp. 669-674.

[9] S.L. Roberson, D. Finello, R.F. Davis, Electrochemical evaluation of molybdenum nitride electrodes in H2SO4 electrolyte, J. Appl. Electrochem., 29 (1999) 75-80.

[10] Y.G. Zhu, X.L. Li, H.L. Wang, J.B. He, D.R. Lu, Technical conditions of preparation and the electrochemical behavior of the film electrode of molybdenum nitride, J. Inorg. Mater., 16 (2001) 1019-1023.
[11] Y.-J. Ting, K. Lian, N. Kherani, Fabrication of Titanium Nitride and Molybdenum Nitride for Supercapacitor Electrode Application, ECS Trans., 35 (2011) 133-139.
[12] B. Cao, J.C. Neuefeind, R.R. Adzic, P.G. Khalifah, Molybdenum Nitrides as Oxygen Reduction Reaction Catalysts: Structural and Electrochemical Studies, Inorg. Chem., 54 (2015) 2128-2136.
[13] M.J. Kim, D.M. Brown, W. Katz, Molybdenum Nitride Film Formation, J. Electrochem. Soc., 130 (1983) 1196-1200.
[14] Z. Samec, K. Doblhofer, Mechanism of Peroxodisulfate Reduction at a Polycrystalline Gold Electrode, J. Electroanal. Chem., 367 (1994) 141-147.
[15] G.N. Botukhova, O.A. Petrii, Electroreduction of peroxodisulfate anion at platinum rotating disc electrode in the cyclic voltammetry mode, Russian Journal of Electrochemistry, 49 (2013) 1145-1153.
[16] K. Inumaru, T. Nishikawa, K. Nakamura, S. Yamanaka, High-pressure synthesis of superconducting molybdenum nitride delta-MoN by in situ nitridation, Chem. Mat., 20 (2008) 4756-4761.
[17] I. Jauberteau, A. Bessaudou, R. Mayet, J. Cornette, J.L. Jauberteau, P. Carles, T. Merle-Mejean, Molybdenum Nitride Films: Crystal Structures, Synthesis, Mechanical, Electrical and Some Other Properties, Coatings, 5 (2015) 656-687.
[18] Y. Honda, S. Fierro, C. Comninellis, Y. Einaga, Influence of Peroxodisulfate Electro-Generation on the Electrochemical Oxidation of Formic Acid on Boron Doped Diamond Electrodes, Meeting Abstracts, The Electrochemical Society, Honolulu, 2012, pp. 3787-3787.
[19] Z. Samec, A.M. Bittner, K. Doblhofer, Electrocatalytic reduction of peroxodisulfate anion on Au(111) in acidic aqueous solutions, J. Electroanal. Chem., 409 (1996) 165-173.
[20] Z. Samec, A.M. Bittner, K. Doblhofer, Origin of electrocatalysis in the reduction of peroxodisulfate on gold electrodes, J. Electroanal. Chem., 432 (1997) 205-214.
[21] J. Desilvestro, M.J. Weaver, Redox Mediation Involving Oxide-Films as Examined by Surface-Enhanced Raman-Spectroscopy - Peroxodisulfate Reduction at Oxide-Modified Gold Electrodes, J. Electroanal. Chem., 234 (1987) 237-249.
[22] V. Climent, M.D. Maciá, E. Herrero, J.M. Feliu, O.A. Petrii, Peroxodisulphate reduction as a novel probe for the study of platinum single crystal/solution interphases, J. Electroanal. Chem., 612 (2008) 269-276.
[23] T.G. Nikiforova, O.A. Petrii, Effect of cadmium and lead adatoms on the reduction kinetics of peroxodisulfate anions at platinized platinum in acid solutions, Russian Journal of Electrochemistry, 41 (2005) 118-121.
[24] G. Kokkinidis, D.G. Zatkas, D. Sazou, Electrocatalysis of $S_2O_8^{2-}$ Ion Reduction, J. Electroanal. Chem. and Interfac. Electrochem., 256 (1988) 137-148.
[25] M.F. de Oliveira, R.J. Mortimer, N.R. Stradiotto, Voltammetric determination of persulfate anions using an electrode modified with a Prussian blue film, Microchemical Journal, 64 (2000) 155-159.
[26] K.C. Lin, J.Y. Huang, S.M. Chen, Poly(brilliant cresyl blue) Electrodeposited on Multi-Walled Carbon Nanotubes Modified Electrode and Its Application for Persulfate Determination, Int. J. Electrochem. Sc., 7 (2012) 9161-9173.
[27] C. Provent, W. Haenni, E. Santoli, P. Rychen, Boron-doped diamond electrodes and microelectrode-arrays for the measurement of sulfate and peroxodisulfate, Electrochim. Acta, 49 (2004) 3737-3744.
[28] D. Pletcher, A First Course in Electrode Processes, 2nd ed., The Royal Society of Chemistry, London, 2009.
[29] B.H. Toby, EXPGUI, a graphical user interface for GSAS, Journal of Applied Crystallography, 34 (2001) 210-213.
[30] D.A. Fletcher, R.F. McMeeking, D. Parkin, The United Kingdom Chemical Database Service, Journal of Chemical Information and Computer Sciences, 36 (1996) 746-749.
[31] C.L. Bull, P.F. McMillan, E. Soignard, K. Leinenweber, Determination of the crystal structure of δ-MoN by neutron diffraction, J. Solid State Chem., 177 (2004) 1488-1492.

[32] A.J. Bard, L.R. Faulkner, Electrochemical methods: Fundamentals and Applications, 2nd ed., Wiley, New York, 2001.
[33] S.C. Perry, L.M. Al Shandoudi, G. Denuault, Sampled-Current Voltammetry at Microdisk Electrodes: Kinetic Information from Pseudo Steady State Voltammograms, Anal. Chem., 86 (2014) 9917-9923.
[34] Z. Samec, K. Krischer, K. Doblhofer, Reduction of peroxodisulfate on gold(111) covered by surface oxides: inhibition and coupling between two oxide reduction processes, J. Electroanal. Chem., 499 (2001) 129-135.
[35] S.C. Perry, G. Denuault, Transient study of the oxygen reduction reaction on reduced Pt and Pt alloys microelectrodes: evidence for the reduction of pre-adsorbed oxygen species linked to dissolved oxygen, Phys. Chem. Chem. Phys., 17 (2015) 30005-30012.
[36] S.C. Perry, G. Denuault, The oxygen reduction reaction (ORR) on reduced metals: evidence for a unique relationship between the coverage of adsorbed oxygen species and adsorption energy, Phys. Chem. Chem. Phys., 18 (2016) 10218-10223.
[37] K. Aoki, K. Akimoto, K. Tokuda, H. Matsuda, J. Osteryoung, Linear Sweep Voltammetry at Very Small Stationary Disk Electrodes, J. Electroanal. Chem., 171 (1984) 219-230.